Fluorination Enables Simultaneous Improvements of a Dialkoxybenzene-Based Redoxmer for Nonaqueous Redox Flow Batteries

Sambasiva R. Bheemireddy, [1,2,+] Zhiguang Li, [1,2,3,+] Jingjing Zhang, [1,2,+] Garvit Agarwal, [1,4] Lily A. Robertson, [1,2] Ilya A. Shkrob,[1,2] Rajeev S. Assary, [1,3] Zhengcheng Zhang[1,2] Xiaoliang Wei,[3] Lei Cheng, [1,3] and Lu Zhang [* 1,2]

[1] *Joint Center for Energy Storage Research, Argonne National Laboratory, 9700 South Cass Avenue, Lemont, IL 60439, USA*

[2] *Chemical Sciences and Engineering Division, Argonne National Laboratory, 9700 South Cass Avenue, Lemont, IL 60439-4837, USA*

[3] *Mechanical and Energy Engineering, Indiana University-Purdue University, Indianapolis, IN, United States*

[4] *Materials Science Division, Argonne National Laboratory, 9700 South Cass Avenue, Lemont, IL 60439-4837, USA*

Abstract: Redoxmers or redox-active organic materials, are one critical component for nonaqueous redox flow batteries (RFBs), which hold high promise in enabling the time domain of grid. While tuning redox potentials of redoxmers is a very effective way to enhance energy densities of NRFBs, those improvements often accompany accelerated kinetics of the charged species, undermining stability and cycling performance. Herein, a strategy for designing redoxmers with simultaneous improvements in redox potential and stability is proposed. Specifically, the redoxmer 1,4-di-*tert*-butyl-2,5-bis(2,2,2-trifluoroethoxy)benzene (ANL-C46) is developed by incorporating fluorinated substitutions into the dialkoxybenzene base platform. Compared to the non-fluorinated analogue, ANL-C46 demonstrates not only an increased (~0.41 V) redox potential, but also much-enhanced stability (1.6 times) and cyclability (4 times) evidenced by electron paramagnetic resonance (EPR) kinetic study, H cell and flow cell cycling. In fact, the cycling performance of ANL-C46 is among the best of high potential (>1.0 V vs. Ag/Ag^+) redoxmers ever reported. DFT calculations suggest that while the introduced fluorine

This is the author's manuscript of the article published in final edited form as:

Bheemireddy SR, Li Z, Zhang J, et al. Fluorination Enables Simultaneous Improvements of a Dialkoxybenzene-Based Redoxmer for Nonaqueous Redox Flow Batteries. ACS Appl Mater Interfaces. 2022;14(25):28834-28841. doi:10.1021/acsami.2c04926

substitutions elevate the redox potentials, they also help to depress the decomposition reactions of the charged redoxmers, affording excellent stability. The findings represent an interesting strategy for simultaneously improving energy density *and* stability, which could further prompt the development of high performance redoxmers.

Keywords: Redoxmer; nonaqueous redox flow batteries; electrochemical performance; bulk electrolysis; cycle life; calendar life.

Introduction:

Nonaqueous redox flow batteries (RFBs) are an emerging solution for reliably integrating intermittent renewable energy sources into the grid.[1] Unlike traditional batteries, NRFBs store electricity in the electrolytes containing redox-active materials or redoxmers. Depending on the materials used, these electrolytes afford various intrinsic redox potentials and circulate through the positive and negative compartments for energy conversion. These redoxmers are denoted as catholyte and anolyte redoxmers, the positive and negative charge storing materials, respectively. While the liquid nature of NRFBs enables many unique features, such as decoupled power and energy, ease of scale-up, and low-cost optimization,[2-4] the practical use of NRFBs still hinges on critical technical progression, including development of redoxmers with both high energy density and long cycle life. In fact, engineering redoxmers towards certain redox potentials and high stability has been the most efficient approach for constructing high performance NRFBs. While higher potential catholyte redoxmers and lower potential anolyte redoxmers are desired for high cell voltages and energy densities, [5] redoxmers with better chemical stability (or calendar life) often result in improved cycling performance.[5-7] However, simultaneously extending redox potential and stability is quite challenging. When redoxmers are more energetic, i.e., catholyte redoxmers with higher potentials and anolyte redoxmers with lower potentials, they are more

thermodynamically unstable.[8] While exceptions exist,[8] this has been observed in many redoxmer studies, where the stability is strongly dependent on the thermodynamic measure of the redox potentials.[5, 9, 10] Such constraints limit the choice of redoxmers, and many energy-dense RFB chemistries suffer undermined cycling stability.[11-17] For instance, Yan et al. reported a family of high potential cyclopropenium based catholyte redoxmers and the best cycling performance was obtained from a lower potential molecule with sustainable 150 cycles under 50% state of charge (SOC) while higher potential ones could only provide less than 50 cycles.[18] Therefore, designing redoxmers to overcome this potential-stability constraint is highly desired for constructing high energy and long cycling RFBs.

As one popular family of redoxmers, the dialkoxybenzene derivatives have been extensively studied for various battery related applications including overcharge protection of lithium-ion batteries and as catholyte materials for nonaqueous RFBs.[19-27] When properly designed, these molecules afford perfect electrochemical reversibility even at high redox potentials, which enables their long-lasting functions in various battery applications. 2,5-Di-*tert*-butyl-1-methoxy-4-(2′-methoxyethoxy)benzene (ANL-C2, Figure 1) is one successful example with a redox potential of ~0.65 V (vs. Ag/Ag^+) in acetonitrile (CH_3CN)-based electrolytes and reasonable stability evidenced by extensive RFB cycling experiments.[28-30] However, further increase of the redox potentials of dialkoxybenzene-based redoxmers has been quite challenging due to accompanying stability compromises. Some examples include tetraethyl-2,5-di-*tert*-butyl-1,4-phenylene diphosphate and 1,4-bis[bis(1-methylethyl)phosphinyl]-2,5-dimethoxybenzene, which demonstrated significantly increased redox potentials by incorporating strong electron withdrawing groups but compromised cycling durability.[31, 32]

In this study, we adopt an established fluorination strategy[33-35] to synthesize a high redox potential dialkoxybenzene-based catholyte redoxmer, 1,4-di-*tert*-butyl-2,5-bis(2,2,2-trifluoroethoxy)benzene (ANL-C46, Figure 1). Compared to ANL-C2, the fluorinated molecule not only demonstrates a significantly increased redox potential but also exhibits unexpected excellent kinetic stability and stable cycling performance, making ANL-C46 one of the most promising high potential catholyte redoxmers, and exemplifying a design strategy towards simultaneous improvements.

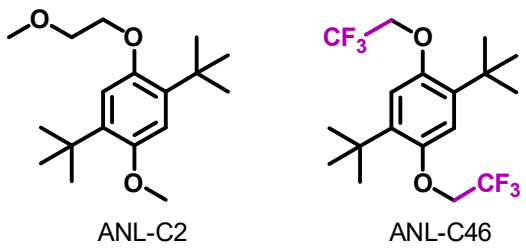

Figure 1. Structures of ANL-C2 and ANL-C46

Results and Discussion:

ANL-C46 was synthesized by a simple Williamson ether synthesis reaction between 2,5-di-*tert*-butylhydroquinone with trifluoro-methanesulfonic acid 2,2,2-trifluoro-ethyl ester in the presence of cesium carbonate (See the Supporting Information for more details). The introduced fluorine atoms are strong electron withdrawing groups, and the carbon fluorine (C-F) bond is very strong. In fact, fluoroalkanes like CF_3- (carbon tetrafluoride) are some of the most unreactive organic groups, which is beneficial to the chemical stability of ANL-C46.

Figure 2 compares the cyclic voltammetry of ANL-C2 and ANL-C46 in an electrolyte of 0.5 M lithium bis(trifluoromethanesulfonyl)imide (LiTFSI) in CH_3CN, and the measured half-wave potentials (calculated by averaging the anodic and cathodic peak voltages), peak current ratios, and diffusion coefficients are summarized in Table S1. As expected, the half-wave potential of

ANL-C46 is 1.06 V vs. Ag/Ag^+, much higher than that of ANL-C2, which is 0.65 V vs. Ag/Ag^+. The > 0.4 V increase indicates that the introduced F atoms are very effective at raising the potentials. Surprisingly, the peak current ratio of ANL-C46 (See Table S1) is closer to 1 compared to that of ANL-C2, indicating a better reversibility of ANL-C46. A long-term CV scan test was also conducted for ANL-C46 (Figure S4c) and after 100 scans, the CV profile remains generally unchanged. In terms of diffusivities, ANL-C2 and C46 are very similar and the solubility of ANL-C46 in the electrolyte is 0.11M.

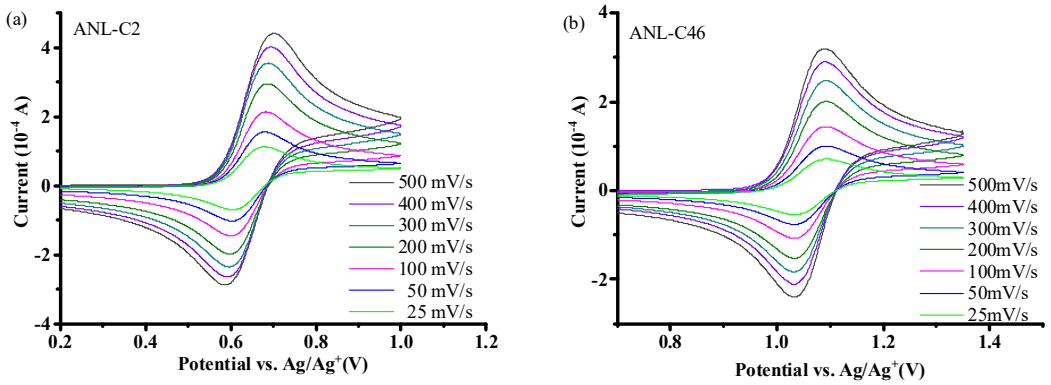

Figure 2. Cyclic voltammograms of 10 mM ANL-C2 (a) and ANL-C46 (b) in CH_3CN at various scan rates from 25–500 mV/s with 0.5 M LiTFSI in CH_3CN.

The kinetic stability of the charged redoxmers (radical cations for dialkoxybenzene-based catholytes) is a crucial parameter to determine the calendar life of RFBs. To this end, the two molecules were charged to 100% state of charge (SOC), and the resultant radical cations were monitored using electron paramagnetic resonance (EPR) spectroscopy (details can be found in the Supporting Information). As shown in Figure 3, the integrated intensities from the EPR spectra were tracked as a function of time to monitor the decay of the radical cations. Despite the higher redox potential, to our surprise, ANL-C46 outperformed ANL-C2 with a much longer half-life time of 275.8 hours (as compared to 163.5 hours for ANL-C2), suggesting an outstanding calendar life. This surprising result is contrary to the intuitive understanding of the thermodynamic-kinetic

relationship that the higher potential catholyte molecules usually have a higher energetic level and a shorter calendar life due to the faster decay.

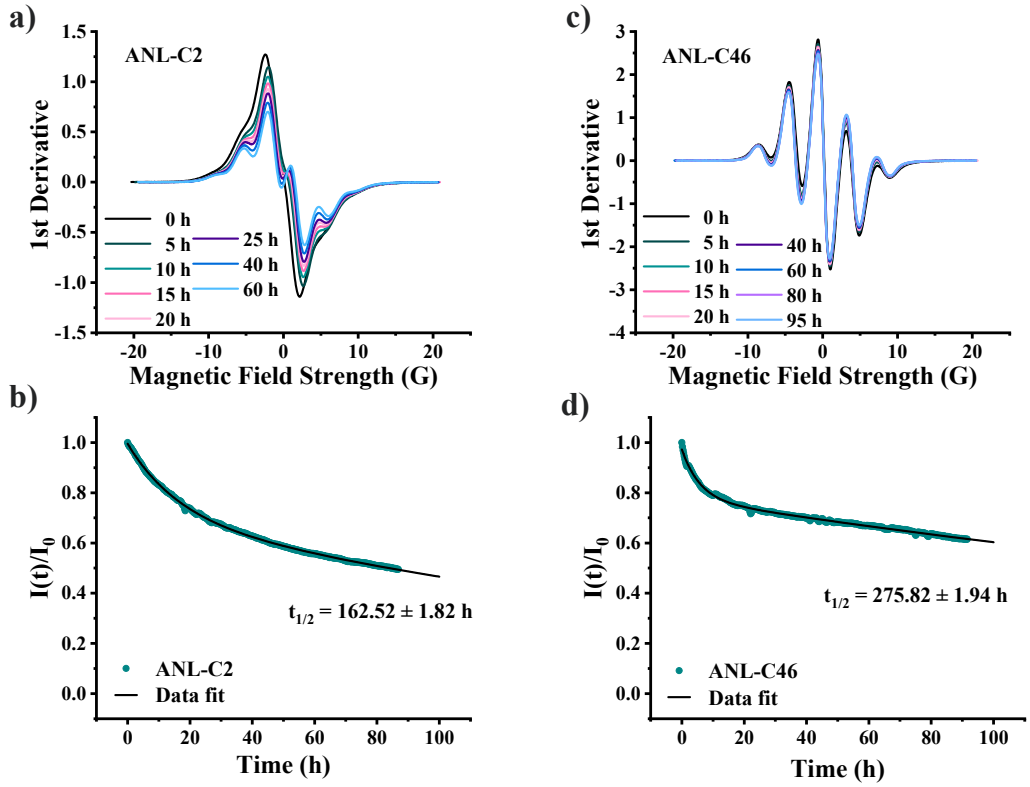

Figure 3. EPR spectra and kinetics profiles for 20 mM ANL-C2$^{\bullet+}$ (a,b) and ANL-C46$^{\bullet+}$ (c,d) in 0.5 M LiTFSI in CH_3CN.

To understand this unexpected enhanced stability of ANL-C46, density-functional theory (DFT) calculations were performed to investigate the structural changes and the possible decay pathways in the charged state. The calculations were performed using Gaussian 16 at the ωb97xD/6-31+G(d,p) level of theory.[36-39] Figure 4 shows the optimized structures of ANL-C2 and ANL-C46 in different oxidation states. As the redoxmers became positively charged from neutral to radical cation, certain bond lengths changed. As shown in Figure 4, the C-O bonds (between the adjacent carbon of benzene ring and first oxygen of the alkoxy chain) became shorter, while the O-C bonds (between the first oxygen and the first carbon of the alkoxyl chain) became longer, suggesting the

de-alkylation of the O-C bonds could be the most likely decomposition pathway of the charged redoxmers. Interestingly, compared to ANL-C2, ANL-C46 exhibited shorter lengths of the O-C bond, implying less favorable de-alkylation pathway.

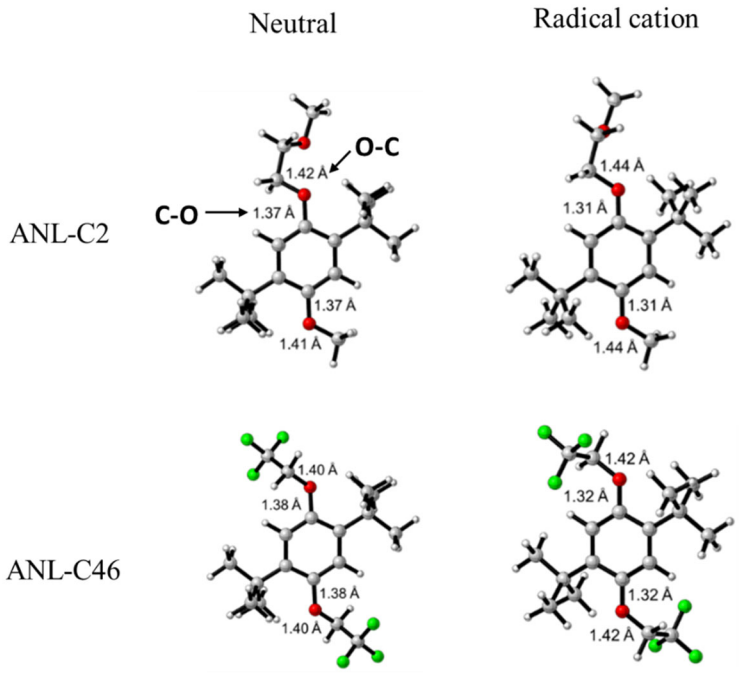

Figure 4. DFT-optimized structures of ANL-C2 and ANL-C46 in their neutral, and radical cation states. The lengths of the C-O (between the adjacent carbon of benzene ring and first oxygen of the alkoxy chain) and O-C (between the first oxygen and the first carbon on the alkoxyl chain) bonds are marked. The C, O, F and H atoms are shown in gray, red, green and white, respectively.

Furthermore, DFT calculations were performed to determine the bond dissociation Gibbs free energies (ΔG) for the possible degradation reactions, including de-protonation and de-alkylation, both of which have been suggested according to previous studies.[22] The computed ΔGs of the reactions and the resulting fragments are summarized in Table 1. The de-methylation ΔG was also computed for ANL-C2. For ANL-C2, the de-alkylation reaction of the O-C bond was the lowest energy pathway with a very low energy of 1.73 kcal/mol, indicating high probability to occur. While for ANL-C46, the energy required to break O-C bond was 34.74 kcal/mol, and the lowest

energy pathway became the de-protonation with a ΔG of 12.68 kcal/mol, still much higher than that of ANL-C2 de-alkylation pathway. Based on those results, the fluorination of ANL-C46 indeed led to significant increase of thermodynamic barrier of decompositions, which may account for the much-improved stability. It was also noted that the computed redox potentials were in good agreement with the experimental values as shown in Table S1, indicating excellent validation of the DFT method.

Table 1. The DFT computed bond dissociation free energies (ΔG, in kcal/mol) of the proposed de-methylation, de-protonation, and dealkylation reactions of ANL-C2 and ANL-C46 cation radicals.

	De-methylation			De-protonation			De-alkylation		
	Frag 1	Frag 2	ΔG	Frag 1	Frag 2	ΔG	Frag 1	Frag 2	ΔG
ANL-C2			(kcal/mol)			(kcal/mol)			(kcal/mol)
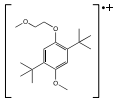	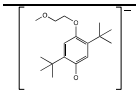	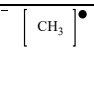	39.26	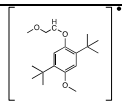	H^+	22.57	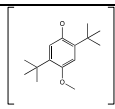	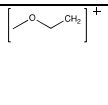	1.73
ANL-C46 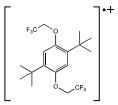	NA	NA	NA	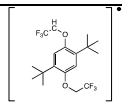	H^+	12.68	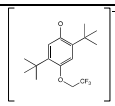	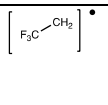	34.74

Next, the cycling stability was tested in a customized H cell containing 5 mL the electrolyte of 20 mM redoxmer and 0.5 M LiTFSI in CH_3CN in each chamber. Details regarding the cycling conditions can be found in the experimental section in the supporting information. The symmetric electrolytes in both working and counter chambers guarantees that the cell cycling is based on reactions of the same redoxmers between neutral and charged states. To eliminate initial side reactions, upon the completion of the first charge, the electrolyte in the counter chamber was

replaced with a fresh one. For each cycle, a capacity control was set to 50% SOC, and the capacity decay would only occur when 50% of redoxmer was consumed or decomposed, which enhanced the contrast for comparison. Figure 5 summarizes the capacity retention and efficiencies profiles of the H-cell cycling for ANL-C2 and ANL-C46. Details can be found in the experimental section. While ANL-C2 exhibited stable capacity retention for 60 cycles, ANL-C46 maintained a stable capacity for over 350 cycles, demonstrating not only significant improvement in cycling stability, but also one of the best performances among all reported high potential (>1.0 V vs Ag/Ag^+) redoxmers.[18, 40, 41] As for the efficiencies, while both molecules maintained a stable coulombic efficiency (CE) throughout the cycling, the energy efficiency (EE) profiles showed a different trend. ANL-C2 had a low but stable EE at ~46% for ~50 cycles, which then decreased as the cycling continued. While the EE values may not be meaningful in a three-electrode setup (cell voltage are recorder as the difference between working and reference electrodes), the changes still demonstrate the cell changes. ANL-C46 exhibited a stable EE value for nearly 300 cycles before a decrease was observed. As shown in the voltage profiles of Figure S5, at the ~50th cycle for ANL-C2 and ~300th cycle for ANL-C46 both of the charging plateaus started to increase at the end of charging step. Both redoxmers suffered low CE for the first cycle, which was related to initial interfacial reactions and is consistent with our previous observations.[42, 43] A post-cycling analysis was conducted by comparing the CV scans of the electrolytes in working and counter chambers before and after the cycling. As shown in Figure S6, while ANL-C46 in the working chamber decreased after cycling as evidenced by the decreased peak current, ANL-C46 was completely decomposed in the counter chamber. We believe that such complete decomposition was due to the uncontrollable potential of the counter electrode. As the counter electrode compensates the charge of the working electrode, its potential can change dramatically and thus

causes accelerated decomposition of redoxmers. We have observed similar behaviors in many H cell cycling. Because of the complete depletion of ANL-C46 in the counter chamber, the redoxmer in the working chamber had to migrate to the counter chamber resulting from the concentration imbalance, causing concentration decrease in the working chamber. This is also a known issue as redoxmer crossover. However, the CV in the working chamber didn't show additional peaks or changed shapes of the curves, indicating the ANL-C46 was quite stable. Those results confirm that while ANL-C46 had a higher redox potential, it could still afford a better cyclicality.

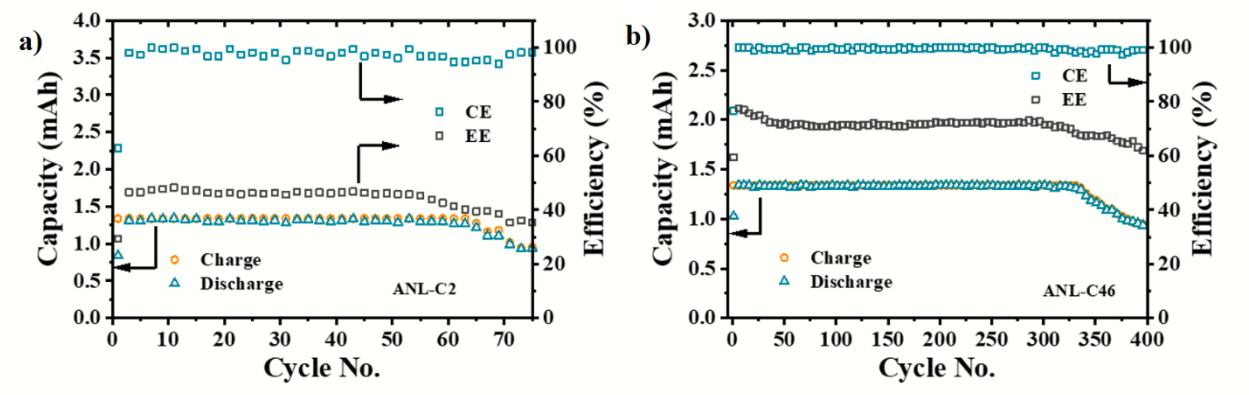

Figure 5. Capacity retention, Coulombic efficiency (CE), energy efficiency (EE) profiles of the H-cell cycling of 20 mM (a) ANL-C2 or (b) ANL-C46 in CH_3CN with 0.5 M LiTFSI. 50% SOC cut-off was used.

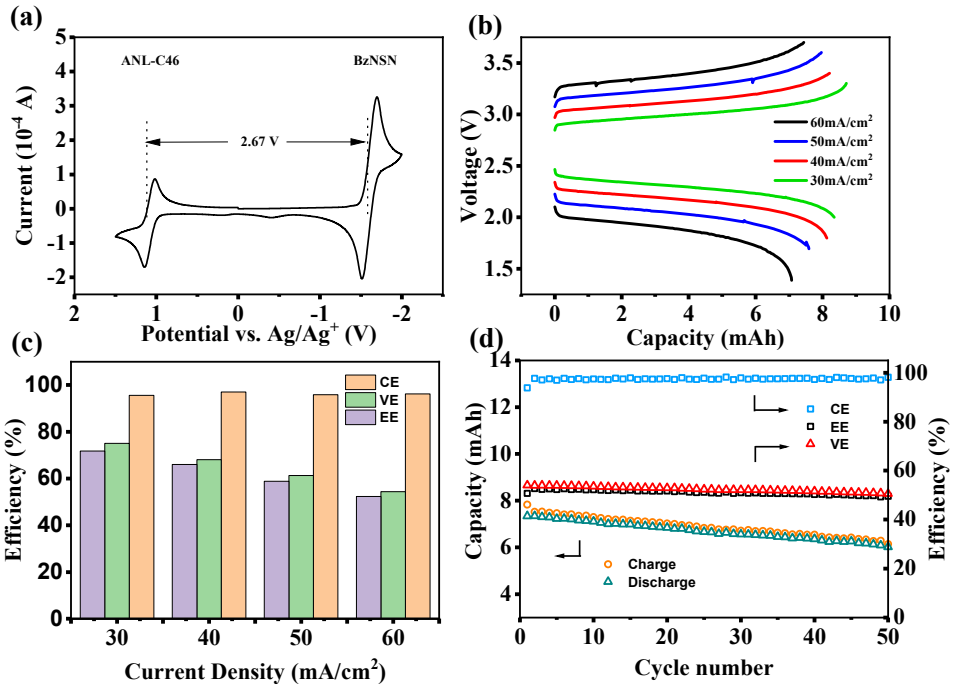

Figure 6. (a) Cyclic voltammograms of 10 mM mixed ANL-C46 and 2,1,3-benzothiadiazole (BzNSN) in CH_3CN at 100 mV/s with 0.5 M LiTFSI. (b-d) Flow cell performance of mixed 0.1 M ANL-C46 and BzNSN in the electrolyte of 1M LiTFSI in CH_3CN. (b)Voltage-capacity profiles and (c) comparison of Coulombic efficiency (CE), voltage efficiency (VE), and energy efficiency (EE) over different current densities; (d) capacity retention and efficiency profiles over 50 cycles at the constant current density of 60 mA/cm^2.

To demonstrate the performance of ANL-C46 in a practical flow cell setting, a low potential anolyte redoxmer, 2,1,3-benzothiadiazole (BzNSN), was used.[5, 8] As shown in the cyclic voltammogram in Figure 6a, a cell voltage of 2.67 V could be achieved when ANL-C46 was coupled with BzNSN in the electrolyte of 0.5 M LiTFSI in CH_3CN. Figure 6b-d summarized the performance of the flow cell containing 0.1 M ANL-C46 and 0.1 M BzNSN cycled at various current densities. As shown in the voltage-capacity profiles (Figure 6b), a smooth charging plateau

at ~2.8-3.1 V and a discharging plateau at ~2.4-2.1 V were observed at 30 mA /cm^2, and the gap between the charging and discharging plateaus became larger as the current density increased due to the increased overpotentials. As a result, the discharge capacities decreased. Such changes were also observed in the efficiency profiles shown in Figure 6c. While the CE values did not change very much, the voltage and energy efficiencies (VE and EE) decreased as cycling current densities increased. The cell was then cycled at the current density of 60 mA/cm^2 for 50 cycles. As shown in Figure 6d, a discharge capacity retention of 83% was obtained (7.38 mAh for 1st cycle and 6.36 mAh for 50th cycle), showing very promising cyclability of the ANL-C46 and BzNSN couple. All efficiencies remained very stable over the cycling at above 99% for CE and 50% for VE and EE. As compared with the reported cycling measures of the ANL-C2 and BzNSN flow cell,[26] the ANL-C46/BzNSN couple delivers a comparable CE but lower VE and EE values. The capacity retention per cycle is at 99.4%, also lower than that of ANL-C2 and BzNSN. A time-based capacity fading profile shown in Figure S6 indicates the capacity decay occurred at 0.46% per minute (Figure S7). One possible reason for this faster decay may be from the difference of the side reactions between charged catholyte and BzNSN. The higher potential of ANL-C46 could lead to more rigorous reaction with BzNSN even though the charged ANL-C46 itself is more stable. In addition, by comparing the voltage profiles of Figure 6b and the Figure S7 in reference 26, the ANL-C46/BzNSN also suffered high overpotentials, which may contribute to the observed lower VE and EE values. However, such hypothesis needs to be verified and we will conduct more comprehensive analysis in the follow-up work.

Conclusion:

The development of redoxmers has been constantly constrained by the often-observed relationship between redox potential and stability. Increasing the redox potential of a catholyte redoxmer leads

to a more energetic charged specie, which may suffer faster kinetic decay or less stability. In this paper, we developed a high potential catholyte redoxmer, ANL-C46, by introducing fluorination to the alkoxy chains that shows a capability of breaking the potential-stability constraint. The strong electron-withdrawing fluorination indeed led to an increased reversible redox potential of $E_{1/2}$ = 1.06 V vs Ag/Ag^+, a > 0.4 V increase compared to that of a well-studied non-fluorinated analogue, ANL-C2. To our surprise, ANL-C46 also afforded a much-enhanced kinetic stability. EPR kinetics study revealed a half-life time of ~275.8 h of the charged ANL-C46, which is much longer than that of the charged ANL-C2 (~162.5 h). The computed bond dissociation free energies (ΔGs) for the possible degradation pathways indicated that the lowest energy decomposition pathway of ANL-C46 should be de-protonation with a ΔG of 12.68 kcal/mol, also much higher than that of ANL-C2, which was the de-alkylation with a ΔG of 1.73 kcal/mol. The H-cell cycling test demonstrated 350 stable cycles of ANL-C46 and a flow cell using mixed ANL-C46 and an anolyte redoxmer, BzNSN, showed a 2.4 V discharge cell voltage and a stable capacity retention (83% for 50 cycles). Designing a redoxmer for NRFB applications requires a comprehensive consideration of multiple properties, including solubility, redox potential, stability, and others,[13] posing a critical challenge for discovering the ideal materials. In this case study, while ANL-C2 is much more soluble,[19] ANL-C46 outperforms in terms of redox potential and kinetic stability, two properties that are often constrained by thermodynamic and kinetic relationship. These findings provide an interesting example of designing catholyte redoxmers with simultaneous improvements of redox potential and stability, which may inspire more strategies toward simultaneous improvements of multiple properties that are desirable for high performance NRFBs.

Experimental:

Materials. 2,5-di-*tert*-butyl-4-methoxy phenol (97%), 2,5-di-*tert*-butylhydroquinone (99%), cesium carbonate (ReagentPlus®, 99%), 2,2,2-Trifluoroethyl trifluoromethanesulfonate (95%), Bis(trifluoromethane)sulfonimide lithium salt (LiTFSI, 99.95% trace metals basis), acetonitrile (CH_3CN, electronic grade, 99.999% trace metal basis) were purchased from Sigma-Aldrich. LiTFSI was dried at 100 ^{0}C under high vacuum overnight before use. ANL-C2 and ANL-C46 were dried by high vacuum at room temperature. The CH_3CN was dried over 3 Å molecular sieves for two days prior to use. All the chemicals were stored in an argon-filled glovebox (O2< 5 ppm, H2O< 0.6 ppm).

The details of syntheses and characterizations of these compounds can be found in the supporting information.

Electrochemical measurements. Cyclic voltammetry of 10 mM redoxmer in CH_3CN containing 0.5 M LiTFSI was obtained using three-electrode configuration with iR compensation at sweep rates ranging from 25 to 500 mV s^{-1} (CHI760D electrochemical workstation CH Instruments, TX). A glassy carbon disk electrode (CHI 104, diameter 3 mm) and Pt wire (CHI 115) were used as working and counter electrodes, and $Ag/AgNO_3$ (10 mM, in CH_3CN) served as a quasi-reference electrode. According to Randles-Sevcik equation, the diffusion coefficient was calculated from $j_p = 2.69 \times 10^5 D^{1/2} v^{1/2} c$, where j_p is the anodic peak current density; D is the diffusion coefficient of the active material (cm^2 s^{-1}); v is the potential sweep rate (V s^{-1}); c is concentration of active material in the bulk electrolyte (mol cm^{-3}). The diffusion coefficient is obtained from the slope of peak current plotted vs. $v^{1/2}$. See Figure 4 in the supporting information for the detailed plots.

The constant-current cycling test was performed in a borosilicate H-cell in an Ar-filled glovebox. The working and counter chambers each contained 5.0 mL of acetonitrile solution (20 mM redoxmer with 0.5 M LiTFSI) that was continuously stirred at 700 rpm min^{-1}. The two chambers

were separated with a porous ceramic disk (P5 frit, Adams and Chittenden). The electrode in each chamber was reticulated vitreous carbon (RVC, 45 PPI, ERG Aerospace Corporation). An $Ag/AgNO_3$ quasi-reference electrode was used on the working side of the H-cell. This cell was cycled to 50% SOC at 8.04 mA (3C rate), with the current reversals occurring at the attainment of the set capacity or potential cutoff limits, whatever comes first. To eliminate degradation products generated during first charge of the H-cell, the electrolyte in the counter electrode chamber was replaced with a fresh solution. The cutoff limits were set to 0 - 1.5 V vs. Ag/Ag^+ for ANL-C2 and 0 - 1.8 V vs. Ag/Ag^+ for ANL-C46 (see Figure S5 in the supporting information for the voltage profiles). The same setup was used to generate radical cations for kinetic studies. For these measurements, the electrolyte was charged at a constant rate of 5C to 100% SOC.

A flow cell consisting of two 2.4cm^2 carbon felt electrodes, a Daramic 800 porous separator, four gaskets, two graphite-made current collectors, and two PVC flow frames was assembled as a sandwich-shape cell to test the electrochemical cycling performance of ANL-C46. Herein, we utilized 1M lithium bis(trifluoromethane sulfonyl) (LiTFSI) and acetonitrile (ACN) as supporting salt and solvent respectively and coupled with 2,1,3-Benzothiadizazole (BzNSN) as anodic redoxmer. In order to mitigate the electrolyte cross-over issue (due to the poor selectivity of Daramic 800), we prepared a 0.1M mixing electrolyte of ANL-C46 and BzNSN. And two glassy vials were loaded with 4ml electrolyte for the anodic and cathodic side individually. The electrolyte was driven by peristaltic pumps with rubber tubes that connect the cell and vials as 27 ml/min. The cell was firstly executed a rate capability test that the current densities were changing from 60 mA/cm^2 to 30 mA/cm^2 and cycled 4 times for each current density. And then its current density was returned to 60 mA/cm^2 to conduct a long cycling test. All of the cyclings were

conducted under constant currents and cut-off voltages were utilized to determine when to stop it. The post-mortem CV was carried out after the electrolyte was diluted 10 times by ACN.

Associated Content:

Supporting Information: Additional experimental details, materials, and methods, including redoxmer synthesis, NMR characterization, EPR characterization, CV, H-cell cycling, flow cell cycling, computational methods, and additional data.

Acknowledgements

This work was financially supported by the Joint Center for Energy Storage Research (JCESR), an Energy Innovation Hub funded by the U.S. Department of Energy, Office of Science, and Basic Energy Sciences. The submitted manuscript has been created by UChicago Argonne, LLC, Operator of Argonne National Laboratory ("Argonne"). Argonne, a U.S. Department of Energy Office of Science laboratory, is operated under Contract No. DE-AC02-06CH11357.

References:

1. Soloveichik, G. L., Flow Batteries: Current Status and Trends. *Chem. Rev.* **2015,** *115* (20), 11533-11558.
2. Soloveichik, G. L., Flow Batteries: Current Status and Trends. *Chem. Rev.* **2015,** *115* (20), 11533-58.
3. Noack, J.; Roznyatovskaya, N.; Herr, T.; Fischer, P., The Chemistry of Redox-Flow Batteries. *Angew Chem Int Edit* **2015,** *54* (34), 9775-9808.
4. Weber, A.; Mench, M.; Meyers, J.; Ross, P.; Gostick, J.; Liu, Q., Redox Flow Batteries: a Review. *J. Appl. Electrochem.* **2011,** *41* (10), 1137-1164.
5. Huang, J.; Duan, W.; Zhang, J.; Shkrob, I. A.; Assary, R. S.; Pan, B.; Liao, C.; Zhang, Z.; Wei, X.; Zhang, L., Substituted Thiadiazoles as Energy-Rich Anolytes for Nonaqueous Redox Flow cells. *Journal of Materials Chemistry A* **2018,** *6* (15), 6251-6254.
6. Huang, J.; Pan, B.; Duan, W.; Wei, X.; Assary, R. S.; Su, L.; Brushett, F. R.; Cheng, L.; Liao, C.; Ferrandon, M. S.; Wang, W.; Zhang, Z.; Burrell, A. K.; Curtiss, L. A.; Shkrob, I. A.; Moore, J. S.; Zhang, L., The Lightest Organic Radical Cation for Charge Storage in Redox Flow Batteries. *Scientific Reports* **2016,** *6* (1), 32102.
7. Zhang, J.; Yang, Z.; Shkrob, I. A.; Assary, R. S.; Tung, S. o.; Silcox, B.; Duan, W.; Zhang, J.; Su, C. C.; Hu, B.; Pan, B.; Liao, C.; Zhang, Z.; Wang, W.; Curtiss, L. A.; Thompson, L. T.; Wei, X.; Zhang, L., Annulated Dialkoxybenzenes as Catholyte Materials for Non-aqueous Redox Flow Batteries: Achieving High Chemical Stability through Bicyclic Substitution. *Advanced Energy Materials* **2017,** *7* (21), 1701272-n/a.

8. Zhao, Y.; Yu, Z.; Robertson, L. A.; Zhang, J.; Shi, Z.; Bheemireddy, S. R.; Shkrob, I. A.; Y, Z.; Li, T.; Zhang, Z.; Cheng, L.; Zhang, L., Unexpected Electrochemical Behavior of an Anolyte Redoxmer in Flow Battery Electrolytes: Solvating Cations Help to Fight against the Thermodynamic–Kinetic Dilemma. *Journal of Materials Chemistry A* **2020,** *8* (27), 13470-13479.
9. Huang, J.; Su, L.; Kowalski, J. A.; Barton, J. L.; Ferrandon, M.; Burrell, A. K.; Brushett, F. R.; Zhang, L., A Subtractive Approach to Molecular Engineering of Dimethoxybenzene-Based Redox Materials for Non-Aqueous Flow Batteries. *Journal of Materials Chemistry A* **2015,** *3* (29), 14971-14976.
10. Kowalski, J. A.; Carney, T. J.; Huang, J.; Zhang, L.; Brushett, F. R., An Investigation on the Impact of Halidization on Substituted Dimethoxybenzenes. *Electrochimica Acta* **2020,** *335*, 135580.
11. Arenas, L. F.; Ponce de León, C.; Walsh, F. C., Redox Flow Batteries for Energy Storage: Their Promise, Achievements and Challenges. *Current Opinion in Electrochemistry* **2019,** *16*, 117-126.
12. Luo, J.; Hu, B.; Hu, M.; Zhao, Y.; Liu, T. L., Status and Prospects of Organic Redox Flow Batteries toward Sustainable Energy Storage. *ACS Energy Letters* **2019,** *4* (9), 2220-2240.
13. Wei, X.; Pan, W.; Duan, W.; Hollas, A.; Yang, Z.; Li, B.; Nie, Z.; Liu, J.; Reed, D.; Wang, W.; Sprenkle, V., Materials and Systems for Organic Redox Flow Batteries: Status and Challenges. *ACS Energy Letters* **2017,** *2* (9), 2187-2204.
14. Chen, H.; Cong, G.; Lu, Y.-C., Recent Progress in Organic Redox Flow Batteries: Active Materials, Electrolytes and Membranes. *Journal of Energy Chemistry* **2018,** *27* (5), 1304-1325.
15. Buhrmester, C.; Moshurchak, L.; Wang, R. L.; Dahn, J. R., Phenothiazine Molecules. *Journal of The Electrochemical Society* **2006,** *153* (2).
16. Kaur, A. P.; Holubowitch, N. E.; Ergun, S.; Elliott, C. F.; Odom, S. A., A Highly Soluble Organic Catholyte for Non-Aqueous Redox Flow Batteries. *Energy Technology* **2015,** *3* (5), 476-480.
17. Milshtein, J. D.; Kaur, A. P.; Casselman, M. D.; Kowalski, J. A.; Modekrutti, S.; Zhang, P. L.; Harsha Attanayake, N.; Elliott, C. F.; Parkin, S. R.; Risko, C.; Brushett, F. R.; Odom, S. A., High Current Density, Long Duration Cycling of Soluble Organic Active Species for Non-aqueous Redox Flow Batteries. *Energy & Environmental Science* **2016,** *9* (11), 3531-3543.
18. Yan, Y.; Robinson, S. G.; Sigman, M. S.; Sanford, M. S., Mechanism-Based Design of a High-Potential Catholyte Enables a 3.2 V All-Organic Nonaqueous Redox Flow Battery. *Journal of the American Chemical Society* **2019,** *141* (38), 15301-15306.
19. Huang, J.; Cheng, L.; Assary, R. S.; Wang, P.; Xue, Z.; Burrell, A. K.; Curtiss, L. A.; Zhang, L., Liquid Catholyte Molecules for Nonaqueous Redox Flow Batteries. *Advanced Energy Materials* **2015,** *5* (6).
20. Zhang, J.; Shkrob, I. A.; Assary, R. S.; Clark, R. J.; Wilson, R. E.; Jiang, S.; Meisner, Q. J.; Zhu, L.; Hu, B.; Zhang, L., An Extremely Durable Redox Shuttle Additive for Overcharge Protection of Lithium-Ion Batteries. *Materials Today Energy* **2019,** *13*, 308-311.
21. Momoe Adachi, K. T., and Koji Sekai, Aromatic Compounds as Redox Shuttle Additives for 4 V Class Secondary Lithium Batteries. *Journal of The Electrochemical Society* **1999,** *146* (4), 1256-1261.
22. Assary, R. S.; Zhang, L.; Huang, J.; Curtiss, L. A., Molecular Level Understanding of the Factors Affecting the Stability of Dimethoxy Benzene Catholyte Candidates from First-Principles Investigations. *The Journal of Physical Chemistry C* **2016,** *120* (27), 14531-14538.
23. Zhang, Z.; Zhang, L.; Schlueter, J. A.; Redfern, P. C.; Curtiss, L.; Amine, K., Understanding the Redox Shuttle Stability of 3,5-Di-tert-butyl-1,2-dimethoxybenzene for Overcharge Protection of Lithium-Ion Batteries. *Journal of Power Sources* **2010,** *195* (15), 4957-4962.
24. Huang, J.; Pan, B.; Duan, W.; Wei, X.; Assary, R. S.; Su, L.; Brushett, F. R.; Cheng, L.; Liao, C.; Ferrandon, M. S.; Wang, W.; Zhang, Z.; Burrell, A. K.; Curtiss, L. A.; Shkrob, I. A.; Moore, J. S.; Zhang, L., The Lightest Organic Radical Cation for Charge Storage in Redox Flow Batteries. *Sci Rep* **2016,** *6*, 32102.

25. Zhang, J.; Shkrob, I. A.; Assary, R. S.; Clark, R. J.; Wilson, R. E.; Jiang, S.; Meisner, Q. J.; Zhu, L.; Hu, B.; Zhang, L. J. M. T. E., An Extremely Durable Redox Shuttle Additive for Overcharge Protection of Lithium-Ion Batteries. **2019,** *13*, 308-311.
26. Duan, W.; Huang, J.; Kowalski, J. A.; Shkrob, I. A.; Vijayakumar, M.; Walter, E.; Pan, B.; Yang, Z.; Milshtein, J. D.; Li, B.; Liao, C.; Zhang, Z.; Wang, W.; Liu, J.; Moore, J. S.; Brushett, F. R.; Zhang, L.; Wei, X., "Wine-Dark Sea" in an Organic Flow Battery: Storing Negative Charge in 2,1,3-Benzothiadiazole Radicals Leads to Improved Cyclability. *ACS Energy Letters* **2017,** *2* (5), 1156-1161.
27. Zhang, L.; Zhang, Z.; Redfern, P. C.; Curtiss, L. A.; Amine, K., Molecular Engineering towards Safer Lithium-Ion Batteries: a Highly Stable and Compatible Redox Shuttle for Overcharge Protection. *Energy & Environmental Science* **2012,** *5* (8), 8204-8207.
28. Xing, X.; Liu, Q.; Xu, W.; Liang, W.; Liu, J.; Wang, B.; Lemmon, J. P., All-Liquid Electroactive Materials for High Energy Density Organic Flow Battery. *ACS Applied Energy Materials* **2019,** *2* (4), 2364-2369.
29. Yuan, J.; Zhang, C.; Zhen, Y.; Zhao, Y.; Li, Y., Enhancing the Performance of an All-Organic Non-Aqueous Redox Flow Battery. *Journal of Power Sources* **2019,** *443*.
30. Wei, X.; Duan, W.; Huang, J.; Zhang, L.; Li, B.; Reed, D.; Xu, W.; Sprenkle, V.; Wang, W., A High-Current, Stable Nonaqueous Organic Redox Flow Battery. *ACS Energy Letters* **2016,** *1* (4), 705-711.
31. Huang, J.; Azimi, N.; Cheng, L.; Shkrob, I. A.; Xue, Z.; Zhang, J.; Dietz Rago, N. L.; Curtiss, L. A.; Amine, K.; Zhang, Z.; Zhang, L., An Organophosphine Oxide Redox Shuttle Additive that Delivers Long-Term Overcharge Protection for 4 V Lithium-Ion Batteries. *Journal of Materials Chemistry A* **2015,** *3* (20), 10710-10714.
32. Zhang, L.; Zhang, Z.; Wu, H.; Amine, K., Novel Redox Shuttle Additive for High-Voltage Cathode Materials. *Energy & Environmental Science* **2011,** *4* (8), 2858-2862.
33. Moshurchak, L. M.; Lamanna, W. M.; Bulinski, M.; Wang, R. L.; Garsuch, R. R.; Jiang, J.; Magnuson, D.; Triemert, M.; Dahn, J. R., High-Potential Redox Shuttle for Use in Lithium-Ion Batteries. *Journal of The Electrochemical Society* **2009,** *156* (4), A309.
34. Weng, W.; Tao, Y.; Zhang, Z.; Redfern, P. C.; Curtiss, L. A.; Amine, K., Asymmetric Form of Redox Shuttle Based on 1,4-Di-tert-butyl-2,5-dimethoxybenzene. *Journal of The Electrochemical Society* **2013,** *160* (10), A1711-A1715.
35. Kaur, A. P.; Ergun, S.; Elliott, C. F.; Odom, S. A., 3,7-Bis(trifluoromethyl)-N-ethylphenothiazine: a Redox Shuttle with Extensive Overcharge Protection in Lithium-Ion Batteries. *Journal of Materials Chemistry A* **2014,** *2* (43), 18190-18193.
36. Kabalka, G. W.; Varma, M.; Varma, R. S.; Srivastava, P. C.; Knapp, F. F., The Tosylation of Alcohols. *The Journal of Organic Chemistry* **1986,** *51* (12), 2386-2388.
37. Chai, J.-D.; Head-Gordon, M., Long-Range Corrected Hybrid Density Functionals with Damped Atom–Atom Dispersion Corrections. *Physical Chemistry Chemical Physics* **2008,** *10* (44), 6615-6620.
38. Rassolov, V. A. R., M. A.; Pople, J. A.; Redfern, P. C.; Curtiss, L. A.,, 6-31G* Basis Set for Third-Row Atoms. *Journal of Computational Chemistry* **2001,** *22* (9), 976-984.
39. Frisch, M. J. T., G. W.; Schlegel, H. B.; Scuseria, G. E.; Robb, M. A.; Cheeseman, J. R.; Scalmani, G.; Barone, V.; Petersson, G. A.; Nakatsuji, H.; Li, X.; Caricato, M.; Marenich, A. V.; Bloino, J.; Janesko, B. G.; Gomperts, R.; Mennucci, B.; Hratchian, H. P.; Ortiz, J. V.; Izmaylov, A. F.; Sonnenberg, J. L.; Williams; Ding, F.; Lipparini, F.; Egidi, F.; Goings, J.; Peng, B.; Petrone, A.; Henderson, T.; Ranasinghe, D.; Zakrzewski, V. G.; Gao, J.; Rega, N.; Zheng, G.; Liang, W.; Hada, M.; Ehara, M.; Toyota, K.; Fukuda, R.; Hasegawa, J.; Ishida, M.; Nakajima, T.; Honda, Y.; Kitao, O.; Nakai, H.; Vreven, T.; Throssell, K.; Montgomery Jr., J. A.; Peralta, J. E.; Ogliaro, F.; Bearpark, M. J.; Heyd, J. J.; Brothers, E. N.; Kudin, K. N.; Staroverov, V. N.; Keith, T. A.; Kobayashi, R.; Normand, J.; Raghavachari, K.; Rendell, A. P.; Burant, J. C.; Iyengar, S. S.; Tomasi, J.; Cossi, M.; Millam, J. M.; Klene, M.; Adamo, C.; Cammi, R.; Ochterski, J. W.; Martin, R. L.; Morokuma, K.; Farkas, O.; Foresman, J. B.; Fox, D. J. , Gaussian 16 Rev. C.01. Wallingford, CT, 2016.

40. Yan, Y.; Robinson, S. G.; Vaid, T. P.; Sigman, M. S.; Sanford, M. S., Simultaneously Enhancing the Redox Potential and Stability of Multi-Redox Organic Catholytes by Incorporating Cyclopropenium Substituents. *Journal of the American Chemical Society* **2021,** *143* (33), 13450-13459.
41. Romadina, E. I.; Volodin, I. A.; Stevenson, K. J.; Troshin, P. A., New Highly Soluble Triarylamine-Based Materials as Promising Catholytes for Redox Flow Batteries. *Journal of Materials Chemistry A* **2021,** *9* (13), 8303-8307.
42. Jingjing Zhang, Z. Y., Ilya A. Shkrob, Rajeev S. Assary, Siu on Tung, Benjamin Silcox, Wentao Duan, Junjie Zhang, Chi Cheung Su, Bin Hu, Baofei Pan, Chen Liao, Zhengcheng Zhang, Wei Wang, Larry A. Curtiss, Levi T. Thompson, Xiaoliang Wei, Lu Zhang, Annulated Dialkoxybenzenes as Catholyte Materials for Non-aqueous Redox Flow Batteries: Achieving High Chemical Stability through Bicyclic Substitution. *Advanced Energy Materials* **2017,** *7*, 1701272.
43. Jinhua Huang, Z. Y., Murugesan Vijayakumar, Wentao Duan, Aaron Hollas, Baofei Pan, Wei Wang, Xiaoliang Wei, and Lu Zhang, A Two-Electron Storage Nonaqueous Organic Redox Flow Battery. *Advanced Sustainable Systems* **2018,** *2*, 1700131.

TOC

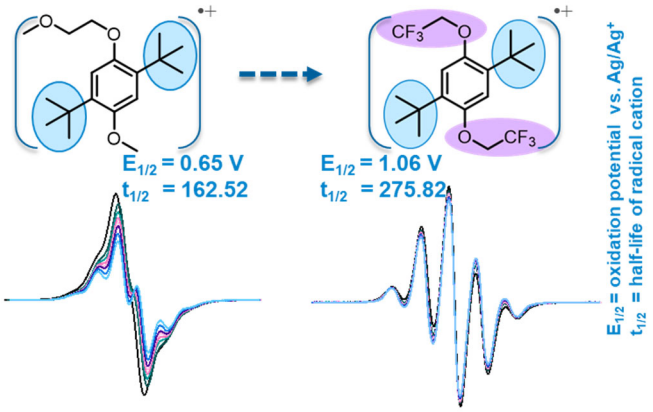
E1/2 = 0.65 V
t1/2 = 162.52
E1/2 = 1.06 V
t1/2 = 275.82
CF3
CF3
E1/2 = oxidation potential vs. Ag/Ag+
t1/2 = half-life of radical cation